AFRL-RX-WP-TP-2011-4289

MECHANICAL PROPERTIES OF $Nb_{25}Mo_{25}Ta_{25}W_{25}$ AND $V_{20}Nb_{20}Mo_{20}Ta_{20}W_{20}$ REFRACTORY HIGH-ENTROPY ALLOYS (PREPRINT)

D.B. Miracle

Metals Branch
Metals, Ceramics, and NDE Division

O.N. Senkov and J.M. Scott

UES, Inc.

G.B. Wilks

General Dynamics Corporation

JULY 2011

AIR FORCE RESEARCH LABORATORY
MATERIALS AND MANUFACTURING DIRECTORATE
WRIGHT-PATTERSON AIR FORCE BASE, OH 45433-7750
AIR FORCE MATERIEL COMMAND
UNITED STATES AIR FORCE

REPORT DOCUMENTATION PAGE

Form Approved
OMB No. 0704-0188

1. REPORT DATE *(DD-MM-YY)*	2. REPORT TYPE	3. DATES COVERED *(From - To)*
July 2011	Journal Article Preprint	01 July 2011 – 01 July 2011

4. TITLE AND SUBTITLE

MECHANICAL PROPERTIES OF $Nb_{25}Mo_{25}Ta_{25}W_{25}$ AND $V_{20}Nb_{20}Mo_{20}Ta_{20}W_{20}$ REFRACTORY HIGH-ENTROPY ALLOYS (PREPRINT)

5a. CONTRACT NUMBER
In-house

5b. GRANT NUMBER

5c. PROGRAM ELEMENT NUMBER
62102F

6. AUTHOR(S)

D.B. Miracle (AFRL/RXLM)
O.N. Senkov and J.M. Scott (UES, Inc.)
G.B. Wilks (General Dynamics Corporation)

5d. PROJECT NUMBER
4347

5e. TASK NUMBER
20

5f. WORK UNIT NUMBER
LM10512P

7. PERFORMING ORGANIZATION NAME(S) AND ADDRESS(ES)

Metals Branch (AFRL/RXLM)
Metals, Ceramics, and NDE Division
Air Force Research Laboratory, Materials and Manufacturing Directorate
Wright-Patterson Air Force Base, OH 45433-7750
Air Force Materiel Command, United States Air Force

UES, Inc.
Dayton, OH 45432

General Dynamics Corporation
Dayton, OH 45431

8. PERFORMING ORGANIZATION REPORT NUMBER
AFRL-RX-WP-TP-2011-4289

9. SPONSORING/MONITORING AGENCY NAME(S) AND ADDRESS(ES)

Air Force Research Laboratory
Materials and Manufacturing Directorate
Wright-Patterson Air Force Base, OH 45433-7750
Air Force Materiel Command
United States Air Force

10. SPONSORING/MONITORING AGENCY ACRONYM(S)
AFRL/RXLM

11. SPONSORING/MONITORING AGENCY REPORT NUMBER(S)
AFRL-RX-WP-TP-2011-4289

12. DISTRIBUTION/AVAILABILITY STATEMENT
Approved for public release; distribution unlimited.

13. SUPPLEMENTARY NOTES
PAO Case Number: 88ABW 2010-5923; Clearance Date: 08 Nov 2010. Document contains color.
Journal article submitted to the *Journal of Alloys and Compounds.*

14. ABSTRACT

Two refractory high entropy alloys with concentrations near $Nb_{25}Mo_{25}Ta_{25}W_{25}$ and $V_{20}Nb_{20}Mo_{20}Ta_{20}W_{20}$, were produced by vacuum arc-melting. Despite containing many constituents both alloys had a single-phase body-centered cubic (BCC) structure that remained stable after exposure to 1400 °C. Compression properties of the alloys were determined in the temperature range of room temperature to 1600 °C. Limited compressive plasticity and quasi-cleavage fracture at room temperature suggests that the ductile-to-brittle transition for these alloys occurs above room temperature. At 600°C and above, both alloys showed extensive compressive plastic strain. The yield strength dropped by 30-40% between room temperature and 600 °C, but was relatively insensitive to temperature above 600 °C . The yield strength values of both alloys were high over the entire temperature range relative to conventional superalloys.

15. SUBJECT TERMS
high entropy alloys, vacuum arc-melting, quasi-cleavage fracture, single-phase body-centered cubic structure

16. SECURITY CLASSIFICATION OF:			17. LIMITATION OF ABSTRACT:	18. NUMBER OF PAGES	19a. NAME OF RESPONSIBLE PERSON (Monitor)
a. REPORT	b. ABSTRACT	c. THIS PAGE			Jonathan E. Spowart
Unclassified	Unclassified	Unclassified	SAR	28	19b. TELEPHONE NUMBER *(Include Area Code)* N/A

Mechanical Properties of $Nb_{25}Mo_{25}Ta_{25}W_{25}$ and $V_{20}Nb_{20}Mo_{20}Ta_{20}W_{20}$ Refractory High-Entropy Alloys

O.N. Senkov[1,2,*], G.B. Wilks[1,3], J.M. Scott[1,2] D.B. Miracle[1]

[1] Air Force Research Laboratory, Materials and Manufacturing Directorate, Wright-Patterson Air Force Base, OH 45433, USA

[2] UES, Inc., Dayton, OH 45432, USA

[3] General Dynamics, Corp., Dayton, OH 45431, USA

ABSTRACT

Two refractory high entropy alloys with concentrations near $Nb_{25}Mo_{25}Ta_{25}W_{25}$ and $V_{20}Nb_{20}Mo_{20}Ta_{20}W_{20}$, were produced by vacuum arc-melting. Despite containing many constituents both alloys had a single-phase body-centered cubic (BCC) structure that remained stable after exposure to 1400°C. Compression properties of the alloys were determined in the temperature range of room temperature to 1600°C. Limited compressive plasticity and quasi-cleavage fracture at room temperature suggests that the ductile-to-brittle transition for these alloys occurs above room temperature. At 600°C and above, both alloys showed extensive compressive plastic strain. The yield strength dropped by 30-40% between room temperature and 600°C , but was relatively insensitive to temperature above 600°C . The yield strength values of both alloys were high over the entire temperature range relative to conventional superalloys.

1. INTRODUCTION

Within the past several years, a new alloying concept, based on achieving high entropy of mixing of alloying elements, has been proposed [1,2,3,4]. According to this experimentally supported concept, high entropy of mixing of different metallic elements (generally ≥5) of near equimolar concentrations can considerably decrease the Gibbs free energy and stabilize solid-solution-like phases with relatively simple crystal structures and a good combination of strength, ductility, thermal stability, oxidation resistance and other properties, rather than forming the conventionally expected complex and brittle intermetallic phases. Using this concept, fundamentally new classes of alloys have recently been developed for structural and functional applications [5,6]. To date, high entropy alloy (HEA) research seems to emphasize alloys based

* Corresponding author. Phone: 937-2551320, e-mail: oleg.senkov@wpafb.af.mil

on the late transition metals such as Cr, Mn, Fe, Co, Ni and Cu. To the authors' knowledge, up to their recent publication [7], there have been no systematic efforts to explore HEAs based primarily on refractory element constituents. Since metallic alloys for high-temperature load-bearing structures and thermal protection remain in high demand for the aerospace industry, there is a clear rationale for exploring HEAs composed of constituents with high melting temperatures.

Two refractory high entropy alloys, $Nb_{25}Mo_{25}Ta_{25}W_{25}$ and $V_{20}Nb_{20}Mo_{20}Ta_{20}W_{20}$, have recently been successfully produced by vacuum arc melting [7]. In the as-cast condition, these alloys have a single-phase body-centered cubic (BCC) crystal structure, with lattice parameters and alloy densities following a rule of mixtures of the alloying elements. A dendritic equiaxed grain structure with the grain size of ~200 μm and 80 μm and very high microhardness of H_v = 4.46 GPa and 5.42 GPa were reported for the four- and five- element alloy, respectively [7]. The aim of the present work was to study the deformation behavior of these refractory alloys in a wide temperature range and compare the properties of these alloys with the properties of superalloys currently used for thermal protection systems and/or gas turbine engines.

2. EXPERIMENTAL PROCEDURES

$Nb_{25}Mo_{25}Ta_{25}W_{25}$ and $V_{20}Nb_{20}Mo_{20}Ta_{20}W_{20}$ alloys, referred to as Alloy 1 and Alloy 2, respectively, were prepared at Pittsburgh Materials Technology, Inc. (Jefferson Hills, PA) by vacuum arc melting of equimolar mixtures of the corresponding elements. High purity Ti was used as a getter for residual gases in the high vacuum chamber. W, Mo, and V were in the form of 45.7 mm diameter rods with a purity of 99.7%, 99.0%, and 99.9% (by weight), respectively, while Ta and Nb were in the form of chips and had a purity of 99.0% and 99.99%, respectively. The alloys were prepared in the form of buttons of ~ 10 mm thick and ~60-70 mm in diameter. To achieve a homogeneous distribution of elements in the alloys, the buttons were re-melted four times, flipped for each melt, and had a total time of over 1 hour in the liquid state. The buttons had lustrous surfaces indicating no oxidation occurred during vacuum arc melting. The final compositios of the alloys, determined by inductively-coupled plasma-optical emission spectroscopy (ICP-OES), are reported in Table 1. Each alloy is close to equiatomic compositions.

Neutron diffraction of the alloys in as-cast and annealed (1400°C for 19 hours) conditions was conducted at the NIST Center for Neutron Research using a high resolution powder diffractometer BT1 (Dr. Mark Green, Instrument Scientist). A Cu(311) monochromator, which produces neutrons with the wavelength of 1.5401 Å, was used. The maximum beam size was 15 mm width x 50 mm height. Before the neutron exposure, the alloy samples of about 10 g each were crushed into powder and loaded in 9.2 mm diameter cylindrical vanadium cans. 32 Helium-3 detectors located at 5^{o} intervals collected scattered neutrons in the 2Θ scan range from 0° to 167°. A CMPR program [8] was used for peak fitting and indexing the neutron diffraction data. Microstructures of as-cast and deformed samples were analyzed with the use of a scanning electron microscope (SEM) equipped with backscatter electron (BSE) detector. Cylindrical specimens for compression testing were electric-discharged machined from the cast buttons. The sample axis was perpendicular to the button surface that was in contact with the copper mold during solidification of the buttons. The samples were ~3.6 mm in diameter and ~ 5.4 mm in height providing the sample aspect ratio of 1.5. The compression faces of the samples were paralleled by mechanical polishing and lubricated with boron nitride (for elevated temperature tests). Compression tests were conducted at temperatures 600°C, 800°C, 1000°C, 1200°C, 1400°C and 1600°C in a computer-controlled Instron (Instron, Norwood, MA) mechanical testing machine outfitted with a Brew vacuum furnace and silicon carbide platens. Prior to each test, the furnace chamber was evacuated to 10^{-6} torr. The sample was then heated to the test temperature in ~45-60 min and soaked at temperature for 15 minutes under 5 N load control, and then compressed to fracture or to a 40% height reduction, whichever occurred first, at a ram speed that provided an initial strain rate of 0.001 s^{-1}. Room temperature compression tests were conducted on the same Instron machine, with the same platen setup and at the same strain rate conditions, but in air, and a thin (~50 μm) Teflon foil was used as a lubricating material between the die and sample contacting surfaces.

3. RESULTS AND DISCUSSIONS

3.1 Mechanical Properties

3.1.1 $Nb_{25}Mo_{25}Ta_{25}W_{25}$ Alloy

The engineering stress vs. engineering strain curves for the $Nb_{25}Mo_{25}Ta_{25}W_{25}$ alloy are given in Figure 1. During compression testing at room temperature (RT, 23°C), the alloy yielded at $\sigma_{0.2}$ =1058 MPa, showed the maximum strength, σ_m, of 1211 MPa at ε_p = 0.95% and failed by splitting at ε_p = 2.1% and σ_f =1135 MPa (Figure 1a). Here ε_p is the plastic strain, $\sigma_{0.2}$ is the yield stress at ε_p = 0.2% and σ_f is the engineering stress at which fracture occurred. The compression modulus, E_{comp}, was determined after the machine compliance correction to be E_{comp} = 220 ± 20 GPa. This resulted in the total elastic strain, ε_e, just before the fracture, of ε_e = 0.52% and the accumulated elastic energy per unit volume W = 2970 ± 270 kJ/m^3.

Samples deformed at T = 600°C and 800°C showed continuous strengthening after yielding at $\sigma_{0.2}$ = 561 MPa and 552 MPa, respectively (Figure 1b). The strengthening rate (and thus the flow stress) at 800°C was higher than at 600°C. The plastic strain exceeded 25% and the peak stress was achieved at the fracture point at 600°C, and at a slightly lower stress at 800°C. The samples deformed at 1000°C, 1200°C and 1400°C reached a peak stress at an intermediate strain, which decreased from ~15% to ~5% with an increase in the temperature, and then their strength continuously decreased. The sample deformed at 1600°C showed almost steady state flow at a constant stress of ~ 590-600 MPa. The yield stress was 548 MPa at 1000°C, 506 MPa at 1200°C, 421 MPa at 1400°C and 405 MPa at 1600°C. The results of compression testing of this alloy are summarized in Table 2.

3.1.2 $V_{20}Nb_{20}Mo_{20}Ta_{20}W_{20}$ Alloy

The engineering stress versus engineering strain curves for the $V_{20}Nb_{20}Mo_{20}Ta_{20}W_{20}$ alloy are given in Figure 2. At RT (Figure 2a), the alloy showed the yield stress $\sigma_{0.2}$ =1246 MPa and the maximum strength σ_m =1270 MPa and failed at ε_p = 1.7% by splitting. The compression modulus was E_{comp} = 180 ± 15 GPa, which resulted in $\varepsilon_e \approx$ 0.60% and W = 3260 ± 330 kJ/m^3 at the fracture point (σ_f =1087 MPa). An increase in the temperature to 600°C decreased the yield stress to $\sigma_{0.2}$ = 862 MPa but increased total compression strain to $\varepsilon_t = \varepsilon_p + \varepsilon_e \approx$ 13% (see Figure 2b and Table 2). With a further increase in the temperature to 1000°C, $\sigma_{0.2}$ slightly decreased to 842 MPa and ε_t increased to 19%. Up to the compression strain of ~5-7%, the deformation

curves of the samples deformed at 600°C, 800°C and 1000°C were almost identical; however, σ_m continuously decreased from 1597 MPa to 1454 MPa.

An increase in the temperature to 1200°C led to a noticeable decrease in $\sigma_{0.2}$ (to 735 MPa), ε_t (to ~8%), and σ_m, (to 943 MPa) (see Figure 2b). A further increase in the temperature to 1400°C and 1600°C led to a considerable softening occurring almost immediately after reaching the yield point. For example, during deformation at T = 1400°C, $\sigma_{0.2}$ was 656 MPa and the peak stress σ_m = 707 MPa was achieved at ε_t = 1.6%; while at T = 1600°C, $\sigma_{0.2}$ = 477 MPa and σ_m, = 479 MPa at ε_t = 0.95%. At these two temperatures, T = 1400°C and 1600°C, the samples did not fracture and the deformation was stopped after ε_t = 18% and 13% resulting in a considerable drop in strength to 200 MPa and 110 MPa, respectively. The results of compression testing of the $V_{20}Nb_{20}Mo_{20}Ta_{20}W_{20}$ alloy are summarized in Table 3.

3.1.3 Comparison with Superalloys

Figure 3 shows the temperature dependence of the yield stress (YS) of the studied HEAs and two high-temperature Ni-based superalloys, Inconel 718 [9] and Haynes 230 [10]. Inconel 718 is a heat treatable alloy and the YS values shown in Figure 3 correspond to heat treatment, which includes annealing at 982°C for1 hour, aging at 718°C for 8 hours, additional aging at 621°C for 18 hours and air cool. After this heat treatment, the YS exceeds 1000 MPa at temperatures up to 650°C. However, the YS of Inconel 718 rapidly decreases to 138 MPa with a further increase in temperature to 982°C, while melting occurs at ~1210°C. Inconel 718 is generally used in gas turbine engines with operating temperatures not exceeding 800°C. Another superalloy, Haynes 230, has a considerably lower YS, which, however, is almost constant, ~255-275 MPa, in the temperature range from 540°C to 870°C. This alloy is non-heat treatable and its applications include hot section components with low loads, such as combustion cans, thermocouple protection tubes, heat exchangers and industrial furnace fixtures, muffles and thermal protection systems operating at temperatures up to 1100°C.

The yield strength values of the refractory HEAs are much higher than that of Haynes 230 at all studied temperatures and higher than that of Inconel 718 at temperatures above 800°C (see Figure 3). Moreover, the decrease in the YS of these HEAs in the temperature range from 600°C to 1600°C is rather weak. For example, YS decreases from 561 to 405 MPa in the

$Nb_{25}Mo_{25}Ta_{25}W_{25}$ alloy and from 862 to 470 MPa in the $V_{20}Nb_{20}Mo_{20}Ta_{20}W_{20}$ alloy in this temperature range.

3.2. Microstructure

3.2.1 Crystal structure

In accord to neutron diffraction analysis, a single-phase BCC crystal structure existing in both high-entropy alloys in the as –cast condition, was also present after annealing at 1400°C for 18 hours (Figure 4). In the $Nb_{25}Mo_{25}Ta_{25}W_{25}$ alloy, the lattice parameter was determined to be a = 3.220 Å, both in as-cast and annealed conditions. In the $V_{20}Nb_{20}Mo_{20}Ta_{20}W_{20}$ alloy, a = 3.185 Å in as-cast condition and a = 3.187 Å in the annealed condition. These results indicate that the BCC crystal structure formed in the alloys during solidification is stable upon heating at least up to 1400°C.

3.2.2 Microstructure in as-cast condition

SEM backscatter electron images of the refractory alloys in as-cast condition are shown in Figure 5. Low magnification images through entire cross-section revealed a non-homogeneous grain structure of the $Nb_{25}Mo_{25}Ta_{25}W_{25}$ alloy, with larger grains at the regions experiencing slower solidification, i.e. near the surfaces not contacting with the water-cooled copper plate (Figure 5a). The average grain size in this alloy was about 200 μm. The $V_{20}Nb_{20}Mo_{20}Ta_{20}W_{20}$ alloy had a much finer grain size, on the order of 80 μm, although the grain size also increased with a decrease in the solidification rate (Figure 5b). Higher magnification images reveal dendritic structure in both alloys (Figure 5c and 5d) Uneven Z-contrast inside the grains indicates slightly different compositions of dendritic and interdendritic regions due to constitutional segregation during solidification [7]. The lighter Z-contrast in both materials indicates that the dendrite arms were enriched with heavier elements than the interdendritic regions. The dendrite arm thickness was about the same in both alloys, ~ 20-30 μm, indicating similar solidification conditions.

3.2.3 Fractography of samples deformed at room temperature

The high entropy alloy samples deformed at room temperature fractured by splitting along the surfaces that were almost parallel to the compression direction. Typical SEM images of the

fracture surfaces are shown in Figure 6. Brittle quasi-cleavage fracture is evident for both alloys. At a low magnification, faceted appearance of the fracture surface is seen (Figure 6 a, b). The size of the facets is finer for the V-containing alloy and is probably correlated to the grain size, as the cleavage planes change directions when they intersect grain or subgrain boundaries. Higher magnification images illustrate characteristics of the quasi-cleavage fracture, such as flat facets, angular faceted steps, river-pattern markings, cleavage feathers and tongues (Figure 6 c-f).

Fracture by splitting suggests that the primary failure mode is tensile, not shear, and that the brittle-to ductile transition temperature (DBTT) is above room temperature for these BCC materials. There are some indications that pores are participating in fracture, but it is not clear that they initiate fracture. Assuming room temperature fracture is cleavage controlled, elastic properties, grain size, and grain boundary character (pores), are critical to controlling toughness. Toughness could also, theoretically be controlled by changes in composition that alter the slip character at low temperatures. Therefore, understanding the deformation mechanisms, and identification of the DBTT for these alloys should be the next step in the research of the deformation behavior of these materials.

3.2.4 Microstructure after deformation at 800°C

SEM backscatter electron images of the samples deformed at 800°C are given in Figure 7. Lower magnification images of the entire cross-sections revealed different deformation behavior of the $Nb_{25}Mo_{25}Ta_{25}W_{25}$ and $V_{20}Nb_{20}Mo_{20}Ta_{20}W_{20}$ alloy samples. Namely, the four-element alloy sample showed a more ductile behavior and it fractured due to localized shear and cracking along a direction inclined about 40° to the loading direction (Figure 7a). Grains inside the shear region were heavily deformed, while no noticeable changes in the grain/dendritic structure (relative to the as-cast condition) were seen in other regions of the sample (Figure 7c). The five-element alloy, on the other hand, was bent, experienced much smaller plastic strain, and its fracture occurred by the crack propagation along the direction inclined 10° to the loading direction (Figure 7b). No noticeable evidence of deformation of grains was observed; however, the grain size slightly increased (to about100-120 μm) in this sample (Figure 7d). The dendritic structure remained in both samples.

3.2.4 Microstructure after deformation at 1400°C

Figure 8 illustrates the microstructure of the $Nb_{25}Mo_{25}Ta_{25}W_{25}$ and $V_{20}Nb_{20}Mo_{20}Ta_{20}W_{20}$ alloy samples after compression at 1400°C. Large grains compressed along the loading direction were clearly seen in the four-element alloy sample, both at low and high magnifications (Figure 8a and 8b). Grains are considerably larger (~300 μm) than in the non-deformed condition indicating strain-induced grain growth. The dendrite arms had the tendency to align almost perpendicular to the loading direction (Figure 8b), which can be an indication of grain rotations and grain boundary sliding. Voids located along grain boundaries also point to grain boundary sliding during compression of this alloy sample.

In contrast, no evidence of grain compression was seen on images of the five-element alloy sample deformed at 1400°C (Figure 8c and 8d). Grains remained equiaxed throughout the sample cross-section, though their size considerably increased to ~150 μm. The equixed morphology of grains after heavy compression is an indication of dynamic recrystallization occurring in this alloy sample during compression. Considerable strain softening (see Figure 2) is another evidence of dynamic recrystallization in the $V_{20}Nb_{20}Mo_{20}Ta_{20}W_{20}$ alloy under these loading conditions [11].

It is interesting to note that the dendritic structure was still present after heavy deformation of both alloys at 1400°C. Even dynamic recrystallization was not able to remove the compositional inhomogeneity. This result supports earlier observations [5,6,12] of heavily reduced diffusivity of elements in high entropy alloys.

4. CONCLUSIONS

Compression testing of two refractory high entropy alloys, $Nb_{25}Mo_{25}Ta_{25}W_{25}$ and $V_{20}Nb_{20}Mo_{20}Ta_{20}W_{20}$ was conducted from room temperature to 1600°C. Neutron diffraction analysis showed that in this temperature range the alloys had a single-phase disordered BCC crystal structure.

During deformation at room temperature, the alloys showed high yield stress of 1058 MPa and 1246 MPa, but a limited ductility of about 2% and 1% of plastic strain, for the 4-component and 5-component alloys, respectively. Quasi-cleavage fracture by splitting along the surfaces that were almost parallel to the compression direction, suggests that fracture occurred under tensile

stresses and that the brittle-to ductile transition temperature for these BCC refractory alloys is above room temperature.

During compression deformation in the temperature range from 600°C to 1600°C, both alloys showed good plastic flow and the plastic compression strain exceeded 20-25% before localized shear accompanied with a drop in strength occurred. In the $Nb_{25}Mo_{25}Ta_{25}W_{25}$ alloy, the yield stress was 561 MPa at 600°C and it continuously decreased to 405 MPa with an increase in temperature to 1600°C. The $V_{20}Nb_{20}Mo_{20}Ta_{20}W_{20}$ alloy was about 200 MPa stronger in the temperature range of 600°C to 1200°C. However, the yield strength of the V-containing alloy decreased more rapidly than the 4-component alloy in the temperature range of 1200°C to 1600°C, so that its yield strength at 1600°C (470 MPa) was close to the yield strength of the 4-component alloy. While near-steady state flow occurred at 1200-1600°C in the 4-component alloy, the 5-component alloy showed considerable softening shortly after the yielding in this temperature range, due to extensive dynamic recrystallization.

5. ACKNOWLEDGEMENTS

Discussions with Drs. Christopher F. Woodward, Patrick L. Martin and Young-Won Kim are greatly appreciated. The authors would like to acknowledge their appreciation of the technical support provided by S.V. Senkova (UES, Inc.) in microstructure analysis. The neutron diffraction was performed at the National Institute of Standard and Technology (Dr. Mark Green). This work was supported by the Air Force Office of Scientific Research (Dr. Joan Fuller, Program Manager) and through USAF Contract No. FA8650-10-D-5226.

TABLES

Table 1. Chemical composition (in wt.% / at.%) of two refractory alloys produced by vacuum arc melting.

Alloy ID / Element	W	Nb	Mo	Ta	V
Alloy 1	36.0 / 27.3	15.2 / 22.7	17.8 /25.6	31.7 / 24.4	0.0 / 0.0
Alloy 2	33.0 / 21.1	16.2 / 20.6	17.6 / 21.7	23.9 / 15.6	9.08 / 21.0

Table 2. Compression properties of the $Nb_{25}Mo_{25}Ta_{25}W_{25}$ alloy.

Temperature °C	Yield Stress MPa	Peak Strength MPa	Peak Strain %	Strength at 25% MPa
23	1058	1211	1.5	1135*
600	561	-	-	1140
800	552	-	-	1283
1000	548	1008	16	763
1200	506	803	12	725
1400	421	467	9	331
1600	405	600	27	597

* Room temperature fracture strength. Fracture occurs at $\varepsilon = 2.6\%$.

Table 3. Compression properties of the $V_{20}Nb_{20}Mo_{20}Ta_{20}W_{20}$ alloy.

Temperature °C	Yield Stress MPa	Peak Strength MPa	Peak Strain %	Fracture Strength MPa	Fracture Strain %
23	1246	1270	0.5	1087	1.7
600	862	1597	13	1597	13
800	846	1536	16	1509	17
1000	842	1454	14	1370	19
1200	735	943	4.2	802	7.5
1400	656	707	1.6	-	-
1600	477	479	0.95	-	-

Table 4. Composition (in wt.%) of Inconel 718 [9].

Ni	Cr	Fe	Mo	Nb	Al	Ti	Co*	Mn*	Cu*	Si*	C*	S*	P*	B*
52	19	Balance	3.0	5.1	0.9	0.3	1.0	0.35	0.5	0.35	0.08	0.015	0.015	0.006

* Maximum.

Table 5. Composition (in wt.%) of Haines 230 [10].

Ni[a]	Cr	Fe*	Mo	W	Co*	Mn	Al	Si	C	La	B*
57	22	3	2	14	5	0.5	0.3	0.4	0.1	0.02	0.015

[a] As Balance; * Maximum

FIGURES

(a)

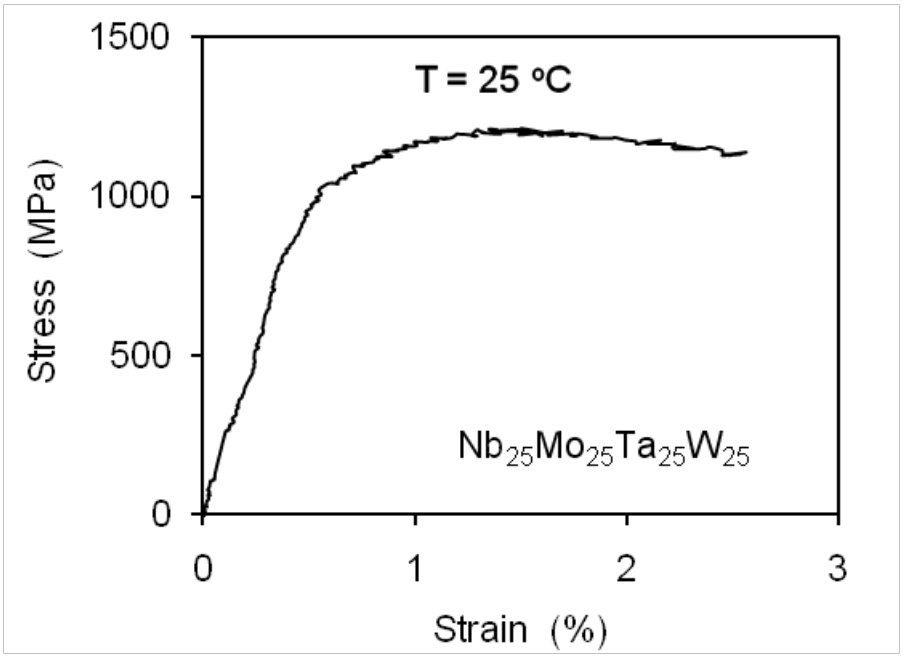

(b)

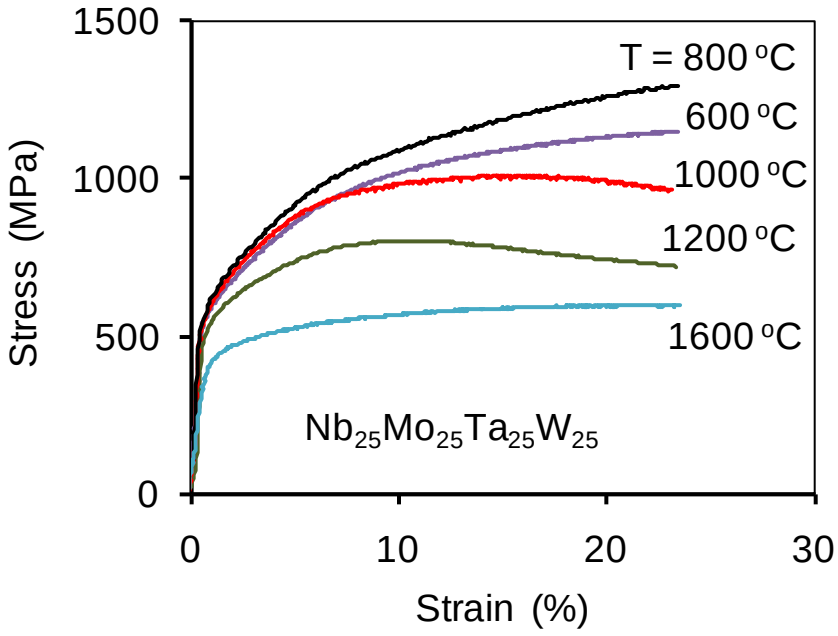

Figure 1. The engineering strain versus engineering stress curves for the $Nb_{25}Mo_{25}Ta_{25}W_{25}$ alloy obtained during compression testing at (a) room temperature and (b) elevated temperatures.

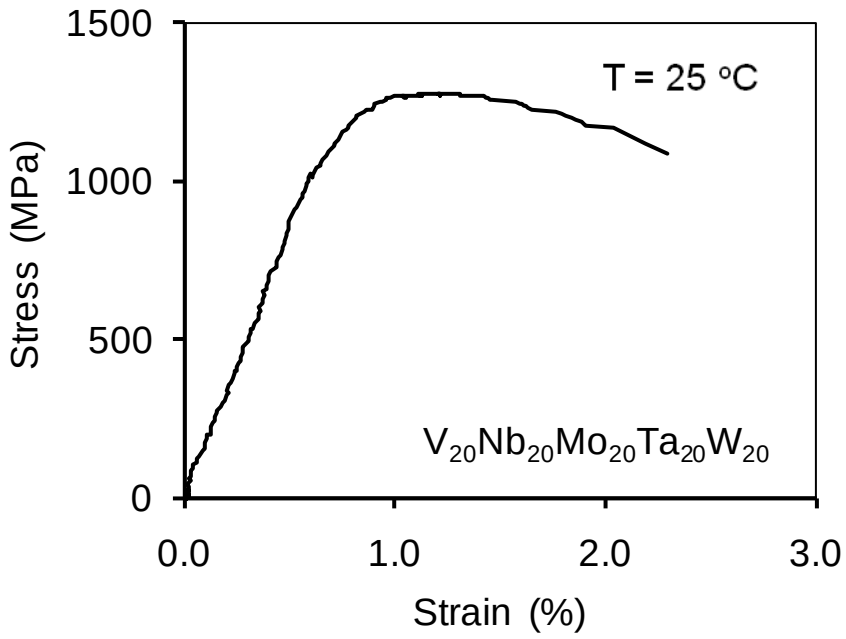

(a)

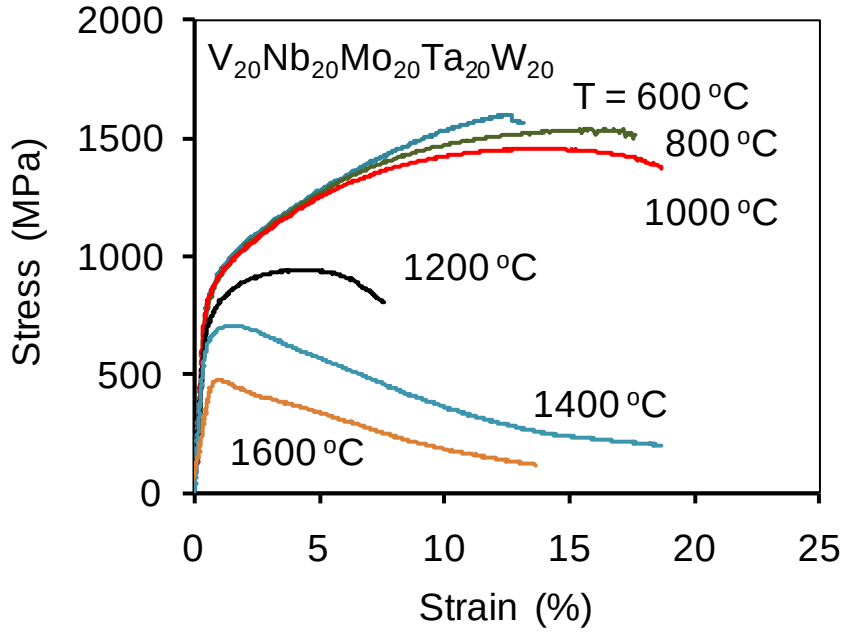

(b)

Figure 2. The engineering strain versus engineering stress curves for the $V_{20}Nb_{20}Mo_{20}Ta_{20}W_{20}$ alloy obtained during compression testing at (a) room temperature and (b) elevated temperatures.

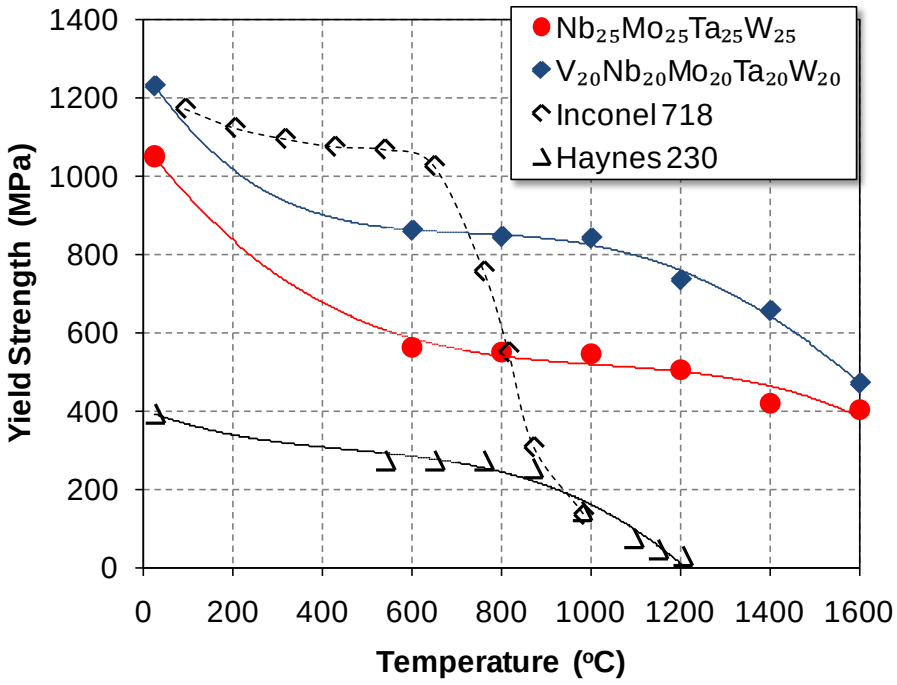

Figure 3. The temperature dependence of the yield strength of $Nb_{25}Mo_{25}Ta_{25}W_{25}$ and $V_{20}Nb_{20}Mo_{20}Ta_{20}W_{20}$ HEAs and two superalloys, Inconel 718 [9] and Haynes 230 [10].

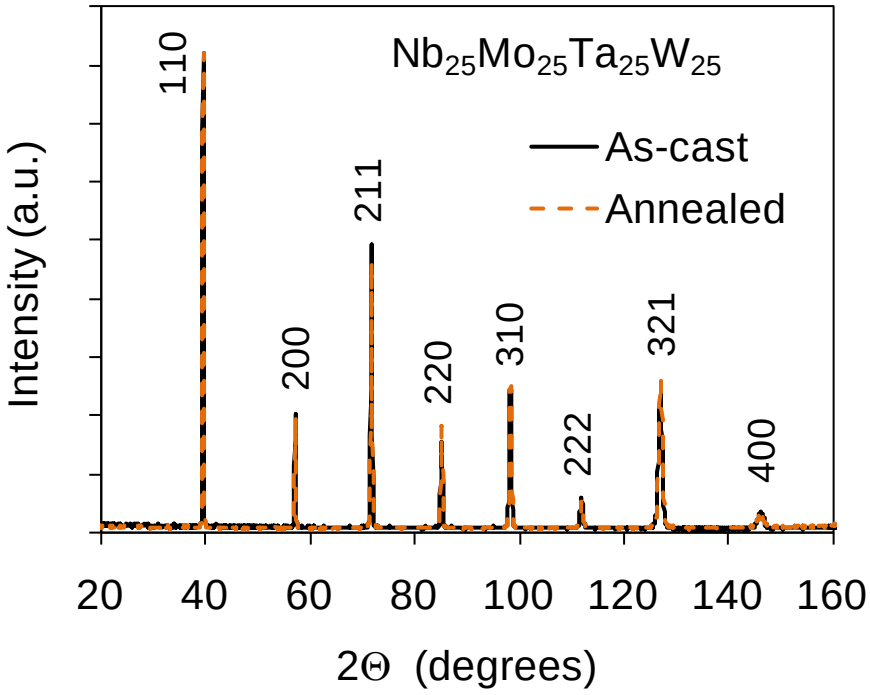

(a)

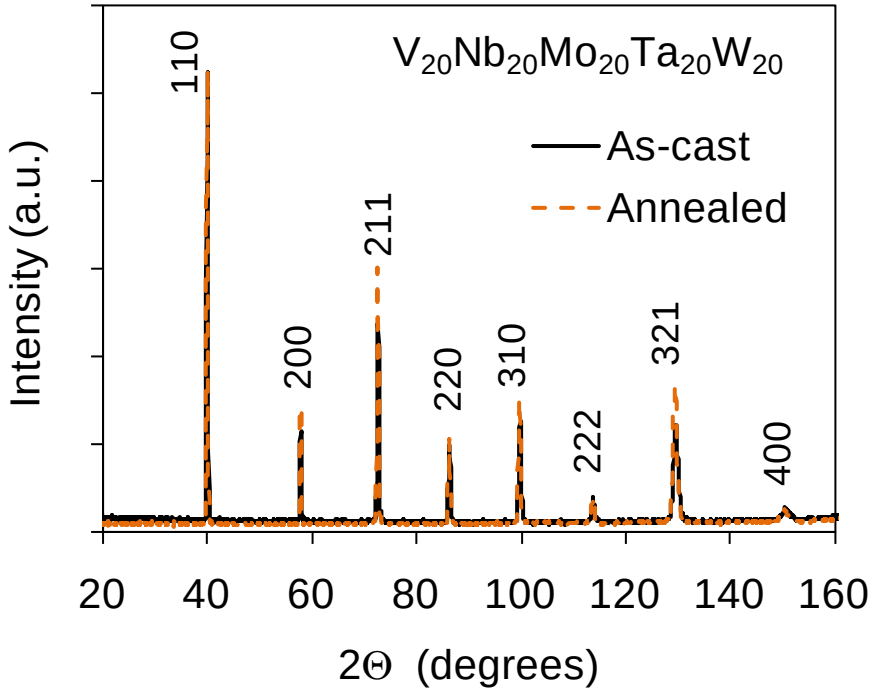

(b)

Figure 4. Neutron diffraction patterns of (a) $Nb_{25}Mo_{25}Ta_{25}W_{25}$ and (b) $V_{20}Nb_{20}Mo_{20}Ta_{20}W_{20}$ in as-cast and annealed (1400°C for 18 hours) conditions. The wavelength is 1.5401 Å.

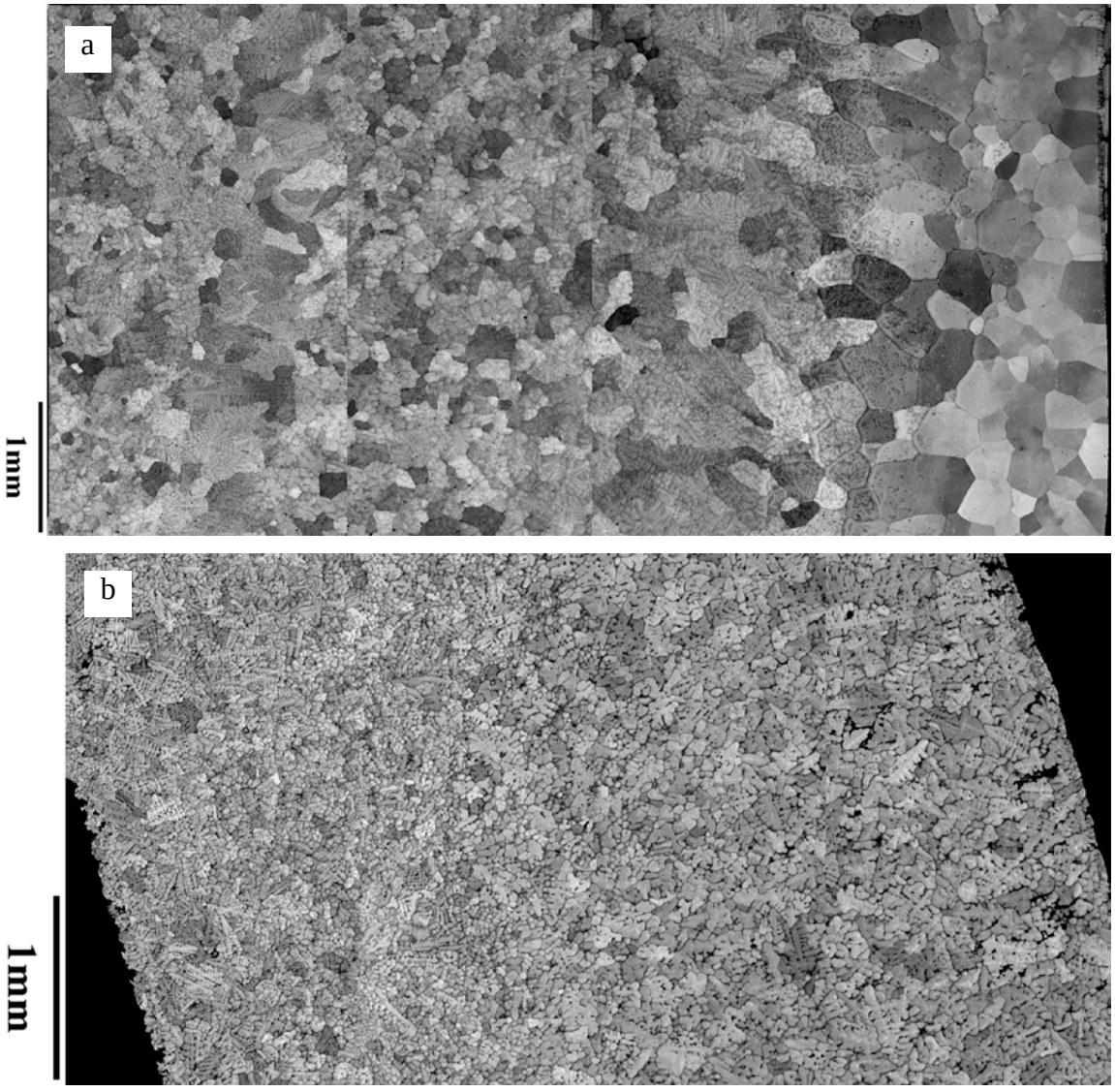

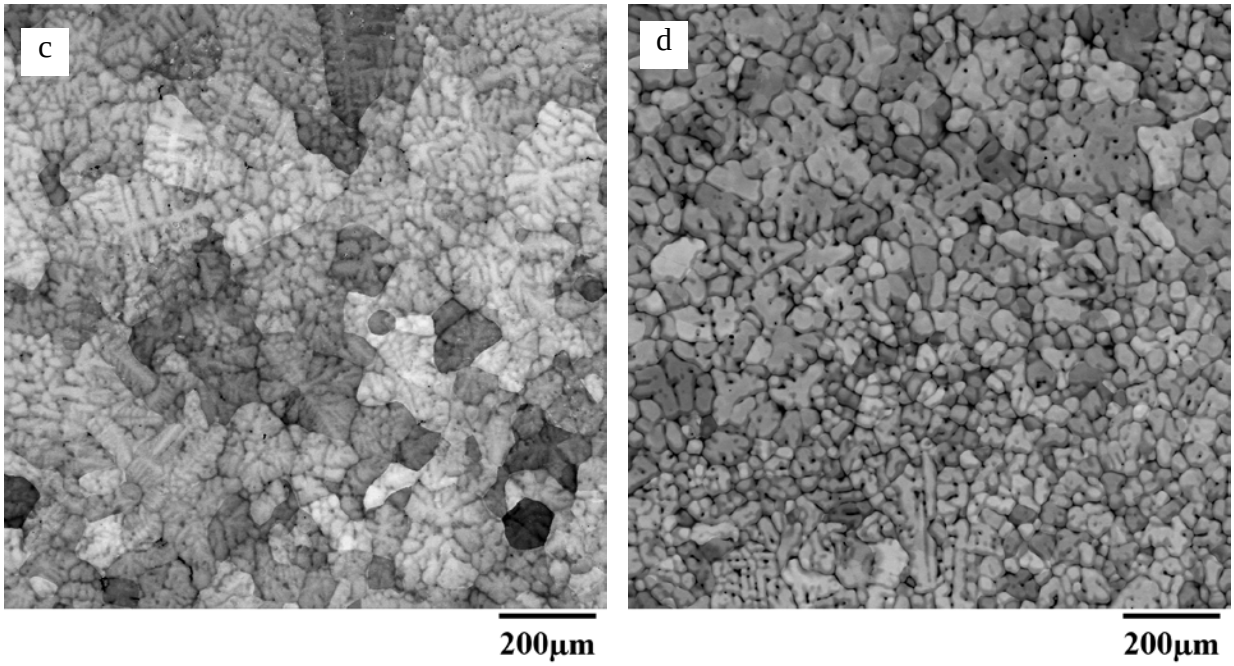

Figure 5: SEM backscatter electron images of a polished cross-section of (a,c) $Nb_{25}Mo_{25}Ta_{25}W_{25}$ and (b,d) $V_{20}Nb_{20}Mo_{20}Ta_{20}W_{20}$ alloys.

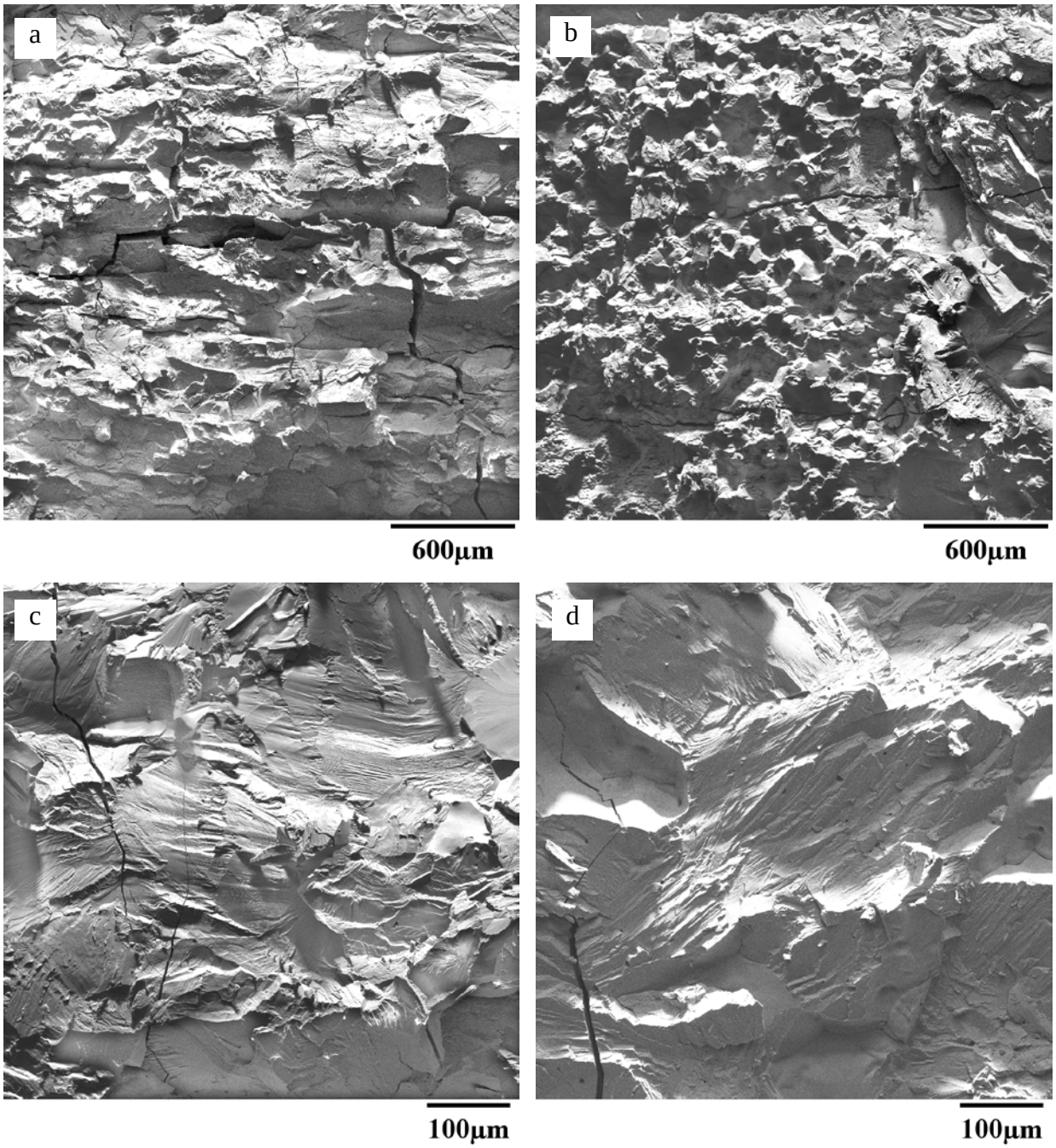

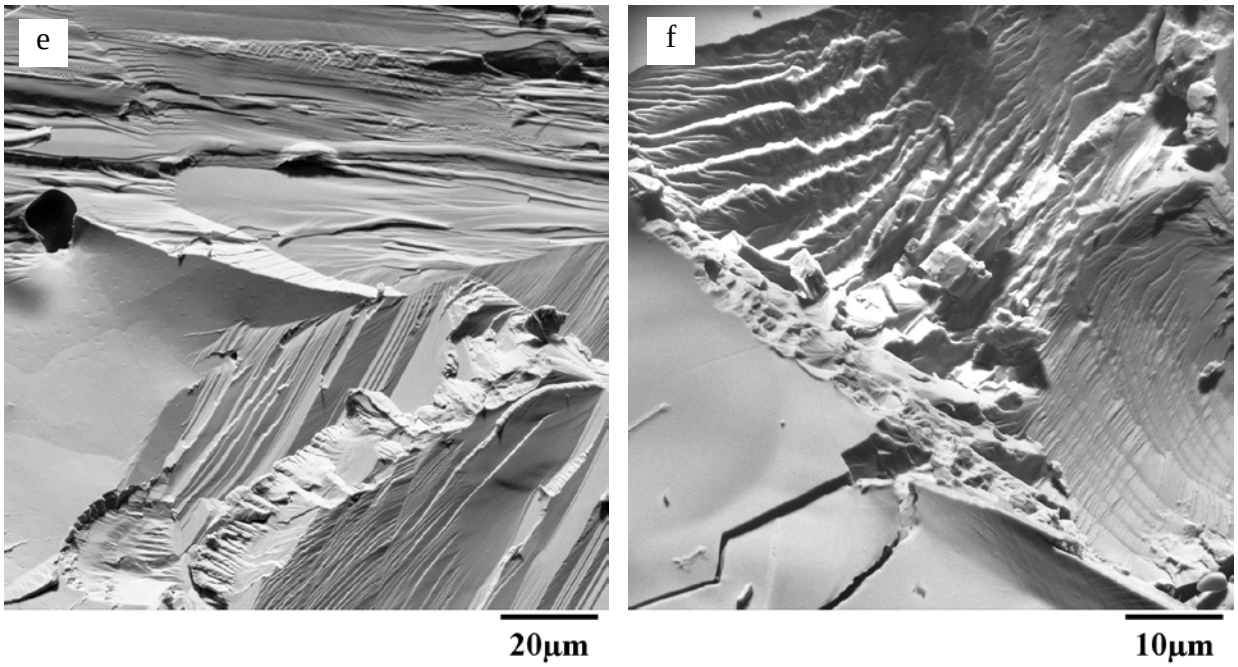

Figure 6. SEM images of fracture surfaces of (a,c,e) $Nb_{25}Mo_{25}Ta_{25}W_{25}$ and (b,d,f) $V_{20}Nb_{20}Mo_{20}Ta_{20}W_{20}$ alloys after compression deformation at 25°C.

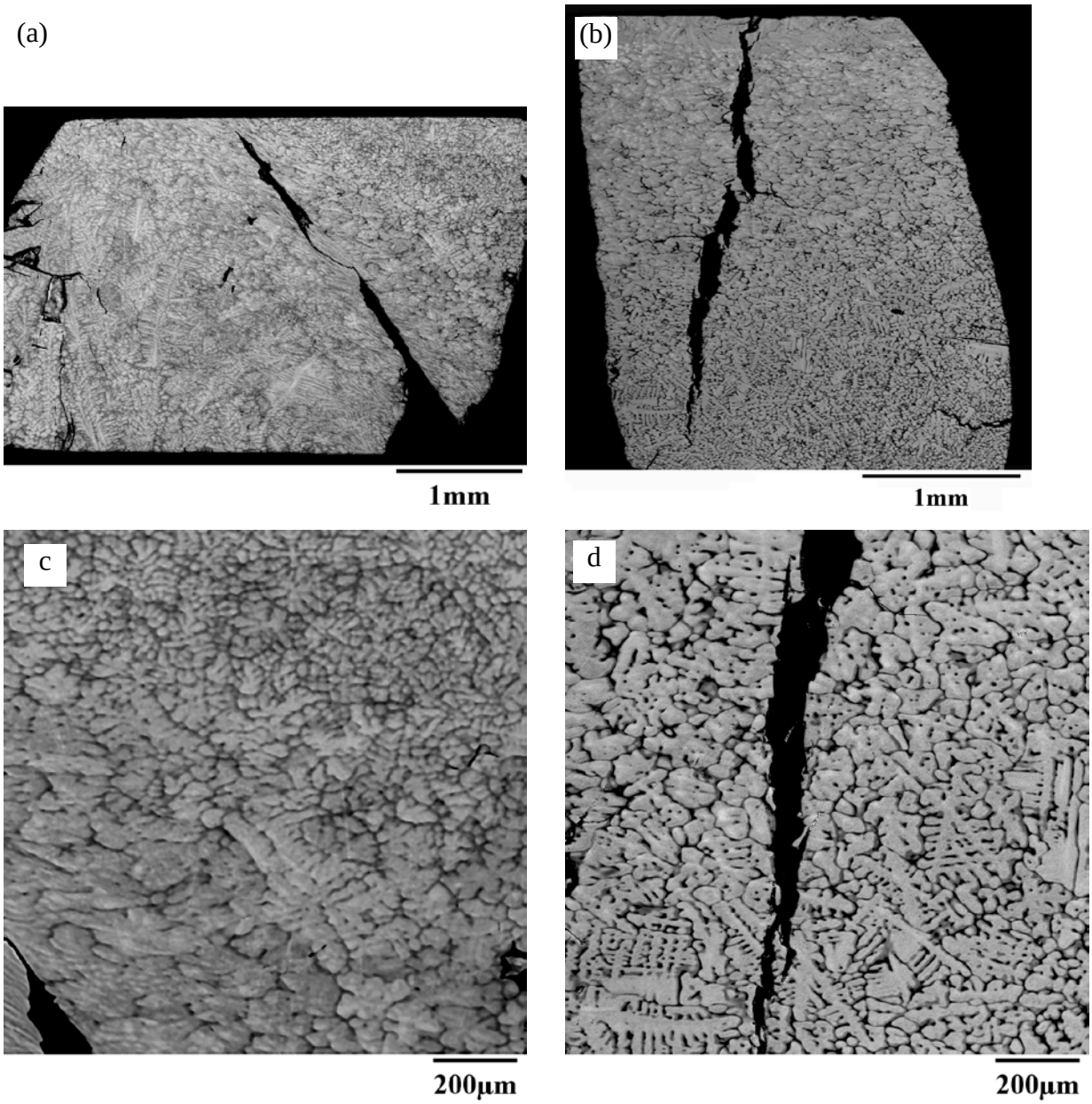

Figure 7. SEM backscatter electron images of the (a,c) $Nb_{25}Mo_{25}Ta_{25}W_{25}$ and (b,d) $V_{20}Nb_{20}Mo_{20}Ta_{20}W_{20}$ alloys after compression deformation at 800°C. The cross-sections are parallel to the loading direction (which is vertical) and located about half distance between the surface and the center of the samples.

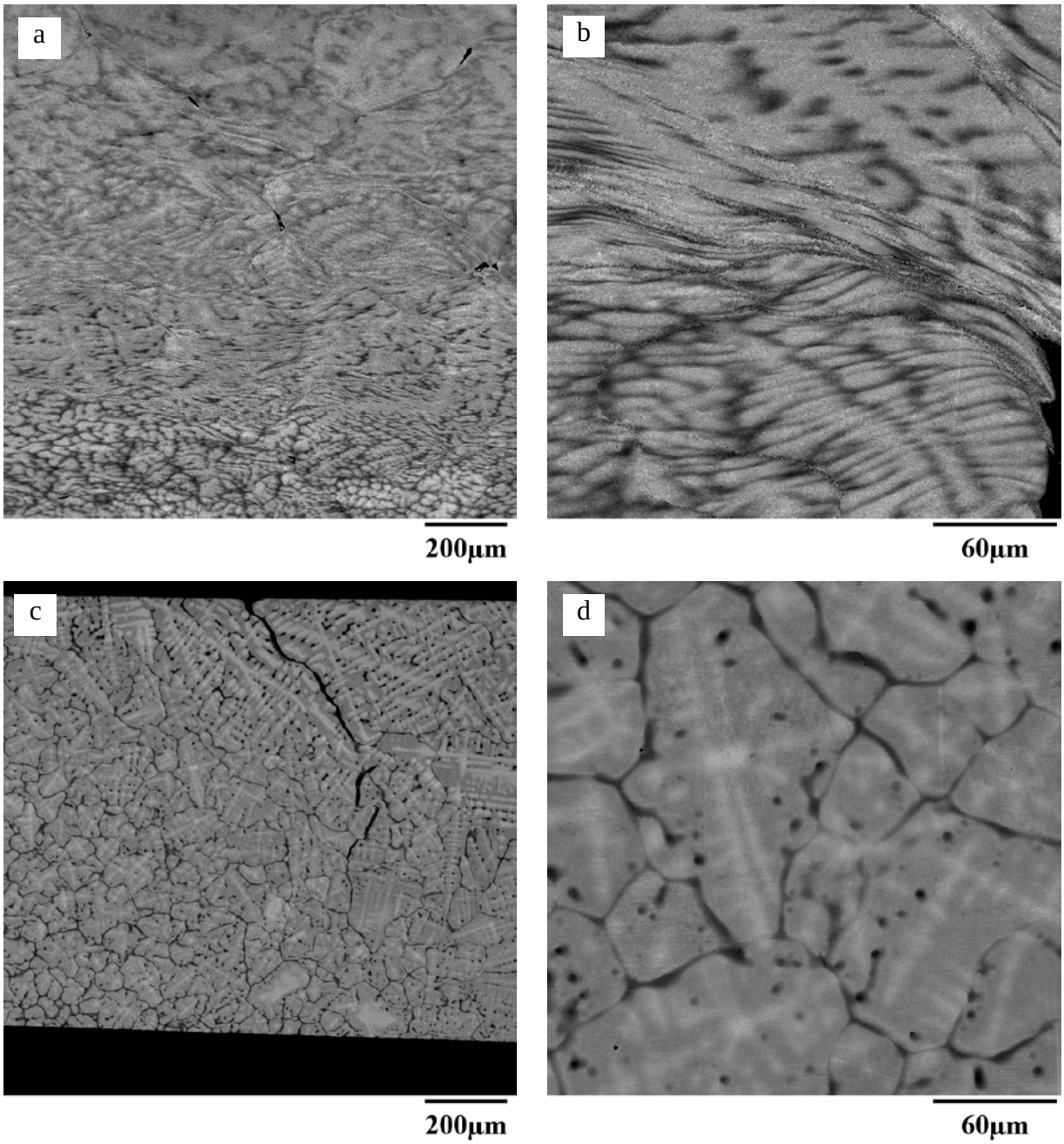

Figure 8. SEM backscatter images of the (a,b) $Nb_{25}Mo_{25}Ta_{25}W_{25}$ and (c,d) $V_{20}Nb_{20}Mo_{20}Ta_{20}W_{20}$ alloys after compression deformation at 1400°C. The cross-sections are parallel to the loading direction (which is vertical) and located about half distance between the surface and the center of the samples.

6. REFERENCES

1 J.W. Yeh, S.K. Chen, S.J. Lin, J.Y. Gan, T.S. Chin, T.T. Shun, C.H. Tsau, S.-Y. Chang, Adv. Eng. Mater., 6(5) (2004) 299-303.

2 P.K. Huang, J.W. Yeh, T.T. Shun, and S.K. Chen, Adv. Eng. Mater., 6(1-2) (2004) 74-78.

3 J.W. Yeh, Ann. Chim. Sci. Mat., 31(6) (2006) 633-648.

4 Y. Zhang,Y.J. Zhou, J.P. Lin, G.L. Chen, P.K. Liaw, Solid-solution phase formation rules for multi-component alloys, Adv. Eng. Mater., 10(6) (2008) 534-538.

5 J.-W. Yeh, Annales de Chimie: Science des Materiaux, 31 (2006) 633-648.

6 J.-W. Yeh, Y.-L. Chen, S.-J. Lin, S.-K. Chen, Mater. Sci. Forum, 560 (2007) 1-9.

7 O.N. Senkov, G.B. Wilks, D.B. Miracle, C.P. Chuang, P.K. Liaw, Intermetallics, 18 (2010) 1758-1765.

8 B.H. Toby, J. Applied Crystallography **38** (2005), 1040-1041.

9 Inconel® Alloy 718, http://www.specialmetals.com/documents/Inconel alloy 718.pdf.

10 Haynes® 230® Alloy, www.haynesintl.com/pdf/h3060.pdf.

11 H.J. McQueen and J.J. Jonas, Treatise on Materials Science and technology, Vol. 6: Plastic Deformation of Materials, Academic Press, New York, 1975, pp.393-493.

12 M.-H. Tsai, J.-W. Yeh, J.-Y. Gan, Thin Solid Films, 516 (2008) 5527-5530.